Ocean Wave Imaging Using an Airborne Single Pass Across-Track Interferometric SAR

Johannes Schulz-Stellenfleth and Susanne Lehner

***Abstract*—An airborne single pass across-track interferometric synthetic aperture radar (InSAR) is used to image ocean waves. A theoretical model explaining the imaging mechanisms is developed, and simulations of the interferogram as well as the conventional SAR intensity image are presented for given ocean wave spectra. Distortions of digital elevation models (DEM) derived from InSAR data are explained by the motion of the sea surface.**

A Monte Carlo method based on forward simulations is used to estimate variance spectra of the distorted elevation models. It is shown that a straightforward estimation of wave height using the distorted InSAR elevation model is in good agreement with true wave height for low amplitude swell with about 10% error depending on propagation direction and coherence time. However, severe underestimation of wave height is found for wind seas propagating in flight direction.

Forward simulations show that the distorted InSAR DEM is less dependent on the model chosen for the real aperture radar mechanism than conventional SAR images.

Data acquired during an experiment over the North Sea by a high precision InSAR system are compared with simulations.

***Index Terms*—Interferometry, ocean waves, synthetic aperture radar (SAR).**

I. Introduction

SO FAR, synthetic aperture radar (SAR) is the only all-weather system providing directional information on ocean waves on a continuous and global basis. For this reason, SAR data have become a valuable source of information for both wave researchers and mariners. SAR imaging of the sea surface has been investigated in many studies [1]–[4]. A major step in understanding the SAR ocean wave imaging process was the derivation of a nonlinear integral transform describing the mapping of a two dimensional ocean wave spectrum into the corresponding SAR image spectrum [1]. Based on this imaging model, algorithms were developed to derive ocean wave spectra from spaceborne SAR observations, using additional information from ocean wave models or buoy measurements [5].

It is well known however, that some care must be taken deriving two-dimensional (2-D) ocean wave spectra from SAR data. Sea surface motion causes unrecoverable information loss during the acquisition process, and incomplete understanding of imaging mechanisms can lead to misinterpretation of SAR scenes [6]. The derivation of sea state parameters like significant wave height from conventional SAR images is based on a model describing the modulation of the radar cross section by ocean waves (real aperture radar modulation). As there is considerable uncertainty in particular about the hydrodynamic part of this modulation mechanism, it is desirable to develop new techniques to obtain wave height information in a more direct way.

In recent years, interest has been growing in interferometric SAR (InSAR) systems, using two SAR antennas to yield additional information on sea surface. So far, studies have been concerned with along track systems with antenna baselines pointing in flight direction [7]. The idea of such a system is to measure motion of the sea surface using the phase difference of two complex SAR images, which have a certain time offset depending on the baseline and the platform velocity. Along track InSAR was successfully used to measure ocean waves [7], ocean currents [8], and scene coherence times [9].

In this study, the ocean wave imaging capability of an across-track InSAR system using two SAR antennas with baseline perpendicular to flight direction is investigated. The idea of such a system is to gain information about the surface elevation by using the phase difference of two complex SAR images, which are acquired at slightly different imaging geometries. These systems are mainly designed to measure high precision digital elevation models of stationary terrain [10]. A spaceborne across-track InSAR will be flown on the space shuttle in 2000 [11].

In this paper, first, a theory describing the across-track InSAR data acquisition process is developed, taking into account sea surface motion. Based on this theory simulations for the elevation model and for the conventional SAR intensity images, acquired by each of the antennas, are carried out. Finally, data acquired in an experiment over the North Sea using the airborne AeS-1 system developed and operated by AeroSensing GmbH [12] are analyzed and compared to simulations.

II. Cross-Track InSAR Ocean Wave Imaging Theory

A single pass across-track InSAR uses two antennas, transmitting and receiving radar signals in turn. The imaging geometry is shown in Fig. 1. The InSAR is moving in the x direction, looking in the negative (right looking) or the positive (left looking) y direction. Each antenna acquires a complex SAR image denoted by i_1 and i_2, respectively. The derivation of a digital elevation model is based on the interferogram I defined by the following expression:

$$I(x,y) = \langle i_1 i_2^* \rangle \tag{1}$$

The asterisk denotes complex conjugation and $\langle\,\rangle$ brackets indicate mean values. Using standard models for the SAR acqui-

Manuscript received April 28, 1999; revised November 10, 1999. This work was supported by the ENVOC Project, German Ministry of Education, Science, and Technology (BMBF).

The authors are with the German Aerospace Center (DLR), IMF, Oberpfaffenhofen, Germany (e-mail: johannes.schulz-stellenfleth@dlr.de).

Publisher Item Identifier S 0196-2892(01)00481-8.

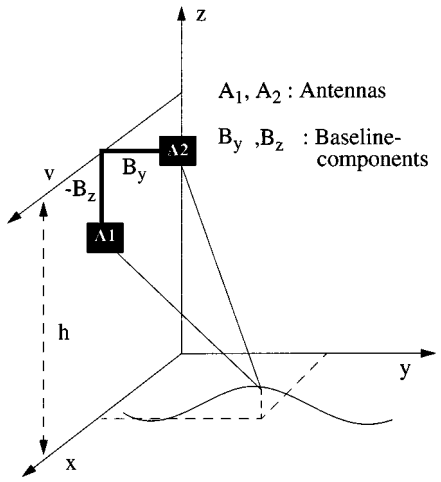

Fig. 1. Imaging geometry of a single pass across-track interferometric SAR (InSAR). The platform is moving in a positive x direction with velocity V.

sition process [7], the formation of the complex images i_1, i_2 can be described as follows:

$$i_{1,2}(x,y) = \int S_{1,2}(t,y)\, \exp\left(ik_E\, \frac{(x-Vt)^2}{R}\right)\, dt. \quad (2)$$

Here, k_E denotes the electromagnetic radar wavenumber V, the platform velocity x and y, the along-track (azimuth) and across-track (range) components, and R is the average distance between radar and imaged area. The acquired raw data $S_{1,2}$ are given by

$$S_{1,2}(t,y) = \int r(x_0,y,t) \cdot \exp(-ik_E R_{1,2}(x_0,y,t))\, G(x_0,t)\, dx_0 \quad (3)$$

with r denoting complex reflectivity of the imaged sea surface. The radar signal roundtrip paths $R_{1,2}$ can be expressed in terms of flight level h, horizontal and vertical component of baseline B_y, B_z, surface elevation z, and time of flight t as follows:

$$R_1(x_0,y_0,t) = 2\sqrt{(h+B_z-z(t))^2+(Vt-x_0)^2+y_0^2} \quad (4)$$

$$R_2(x_0,y_0,t) = 2\sqrt{(h-z(t))^2+(Vt-x_0)^2+(y_0-B_y)^2}. \quad (5)$$

Here, an InSAR system with both antennas transmitting and receiving in turn is assumed. Denoting the SAR integration time by T_0, a standard model for the antenna pattern G is given by the following expression [13]:

$$G(x_0,t) = \exp\left(-2\,\frac{(x_0-Vt)^2}{V^2T_0^2}\right). \quad (6)$$

In the following, the common assumption [2] is made that the complex reflectivity r is uncorrelated in space. Denoting the so-called scene coherence time by τ_s [14], this leads to the following expression for the autocovariance function of the complex reflectivity:

$$\langle r(x_1,y,t_1)\, r^*(x_2,y,t_2)\rangle = \sigma\left(x_1,y,\frac{t_1+t_2}{2}\right)\delta(x_1-x_2) \cdot \exp\left(-\frac{(t_1-t_2)^2}{\tau_s^2}\right) \quad (7)$$

where σ is the radar cross section. Inserting (2) into (1) and integrating over one space dimension yields the following expression for the InSAR interferogram:

$$I(x,y) = \iiint \sigma\left(x_1,y,\frac{t_1+t_2}{2}\right) \cdot \exp\left(-\frac{(t_1-t_2)^2}{\tau_s^2}\right) \cdot \exp(ik_E(R_2(x_1,y,t_2)-R_1(x_1,y,t_1))) \cdot \exp\left(ik_E\,\frac{(x-Vt_1)^2-(x-Vt_2)^2}{R}\right) \cdot \exp\left(-2\,\frac{(x_1-Vt_2)^2+(x_1-Vt_1)^2}{V^2T_0^2}\right) \cdot dx_1\, dt_1\, dt_2. \quad (8)$$

To further simplify this expression, the signal roundtrip path difference $R_2 - R_1$ is expanded to second order in time.

$$R_2(x_1,y,t_1)-R_1(x_1,y,t_2) \approx \Delta R(x_1,y) + \frac{V(t_2-t_1)(V(t_1+t_2)-2x_1)}{R} - 2\,u_r\left(x_1,y,\frac{t_1+t_2}{2}\right)(t_2-t_1) \quad (9)$$

Here ΔR is the signal roundtrip path difference at Doppler zero

$$\Delta R(x_1,y) = 2\sqrt{\left(h-z_0\left(t=\frac{x_1}{V}\right)\right)^2+(y-B_y)^2} - 2\sqrt{\left(h+B_z-z_0\left(t=\frac{x_1}{V}\right)\right)^2+y^2}. \quad (10)$$

The orbital velocity of the backscattering facettes in slant range direction u_r is approximated as

$$u_r(x,y,t) = u_r\left(x,y,t=\frac{x}{V}\right) + a_r\left(x,y,t=\frac{x}{V}\right)\,(t-x/V) \quad (11)$$

with a_r denoting orbital acceleration in slant range direction. Assuming the cross section σ to be constant during integration time, after some algebraic manipulations, the following expression for the interferogram is found:

$$I(x,y) = 0.5\, T_0^2\rho_a\pi \int \frac{\sigma(x_1,y)}{\hat{\rho}_a(x_1,y)} \cdot \exp(ik_E\Delta R(x_1,y))\, \exp\left(-\frac{\pi^2}{\hat{\rho}_a^2(x_1,y)} \cdot \left(x-x_1-\frac{R}{V}\,u_r(x_1,y)\right)^2\right) dx_1. \quad (12)$$

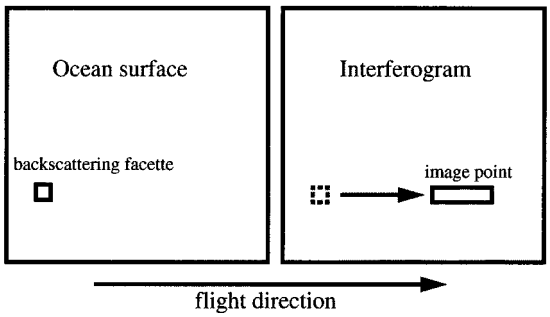

Fig. 2. Due to sea surface motion, complex image points in the across-track InSAR interferogram are shifted and smeared in the azimuth direction.

The following definitions are used in (12). The degraded azimuthal resolution $\hat{\rho}_a$ is

$$\hat{\rho}_a(x_1, y) = \sqrt{\rho_a^2 + \left[\frac{\pi}{2}\,\frac{T_0 R}{V}\,a_r(x_1, y)\right]^2 + \frac{\rho_a^2 T_0^2}{\tau_s^2}} \tag{13}$$

with the azimuthal SAR resolution ρ_a given by

$$\rho_a = \frac{\lambda_E R}{2VT_0}. \tag{14}$$

T_0 is the SAR integration time, and T_a is defined by

$$\frac{1}{T_a^2} = \frac{1}{\tau_s^2} + \frac{1}{T_0^2}. \tag{15}$$

The radar wavelength is $\lambda_E = 2\,\pi/k_E$. Equation (12) describes the mapping of a moving ocean surface into the corresponding across-track interferogram and will be referred to as the forward model in the following. The result is consistent with the models described in [7] and [14], insofar as setting the baseline components B_y, B_z to zero yields identical equations. Furthermore, neglecting the orbital acceleration a_r and the finite SAR resolution yields the forward model for the SAR intensity image used by Hasselmann as the basis for a closed integral transform describing the SAR imaging mechanism in the spectral domain [1].

The basic conclusion to be drawn from (12) is that complex image points in the across-track interferogram are shifted and smeared in the azimuth direction in a way similar to that known from intensity images of a conventional SAR (see Fig. 2. The shift of image points is linearly connected to orbital velocity u_r, whereas the smearing is related to acceleration a_r, scene coherence time τ_s, and integration time T_0. The most dominant system parameter in the nonlinear imaging process is the ratio $\beta = R/V$.

Because of these distortions, the elevation model derived from the interferogram will be referred to as the "bunched DEM" in the following.

III. Ocean Wave Imaging with the AES-1 Cross Track InSAR System

An experiment using across-track InSAR for ocean wave imaging was carried out with the high precision AeS-1 system developed and operated by AeroSensing GmbH [12]. The AeS-1 is an airborne system that can be flown on small airplanes. The main parameters relevant to the imaging process are given in Table I. The full azimuthal resolution of 0.5 m is achieved using an integration time of about 1.8 s. However, to reduce smearing effects caused by sea surface motion (13), only about 0.1 seconds integration time were actually used for processing the data, resulting in a lower azimuthal resolution of about 10 m.

TABLE I
Imaging Parameters of Presented Data Acquisitions by the AES-1 Across-Track InSAR System

Velocity	85 m/s
Height	3100 m
Transmitting frequency	9.5 GHz
Pulse repetition frequency	8000 Hz
V-Baseline	-1.408 m
H-Baseline	-0.68 m
Incidence angle	≈ 45 degre
Polarization	HH
Range resolution	ca. 0.5 m
Azimuth resolution	ca. 0.5 m
R/V	≈ 50 s

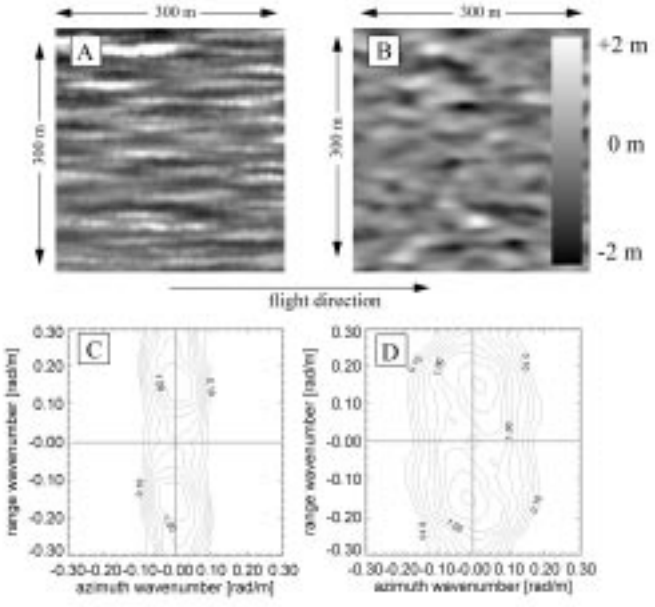

Fig. 3. (a) The 300 m × 300 m SAR intensity image of the ocean surface, (b) corresponding bunched DEM acquired by the InSAR over the North Sea (54°2′N, 8°25′ E) on Feb 6, 1997, (c) spectra of intensity image, and (d) bunched DEM.

Data were acquired over the North Sea near Cuxhaven on February 6, 1997. The plane was flown in southerly direction at 3100 m altitude with a speed of about 85 m/s. Fig. 3(a) shows a 300 m by 300 m subscene of the SAR intensity image acquired by the master antenna and the corresponding bunched DEM (B) with flight direction to the right. The respective spectra Fig. 3(c), (d) show a wave system of about 40 m wavelength in range (across flight) direction. Defining a significant wave height $\overline{HS}$

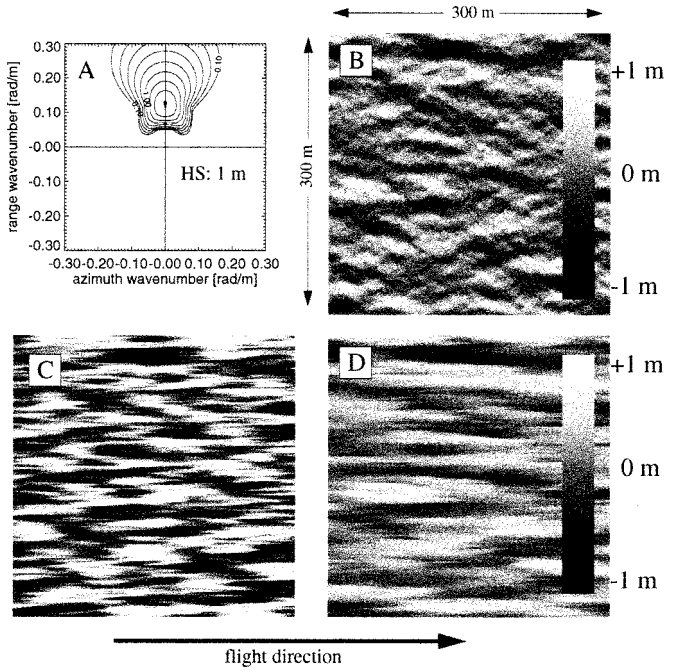

Fig. 4. (a) JONSWAP wind sea spectrum (fully developed) with significant wave height of 1 m corresponding to 7 m/s windspeed, (b) simulated sea surface elevation, (c) simulated SAR intensity image, and (d) simulated bunched DEM.

for the bunched DEM in the same way as for ocean surface elevation, i.e.,

$$\overline{HS} = 4\,\sigma_{\mathrm{DEM}} \tag{16}$$

with standard deviation σ_{DEM}, one obtains $\overline{HS} \approx 1.9$ m for the observed data.

In the next section, we present several simulations and compare them to the observation.

IV. Forward Simulations for Across-Track InSAR

Based on the forward model derived in Section II, simulations for across-track InSAR ocean wave imaging are performed. As *in situ* ocean wave measurements for the InSAR acquisitions near Cuxhaven are not available, a parameterized Joint North Sea Wave Project (JONSWAP) [18] ocean wave spectrum, which describes a fully developed wind sea, was used for the simulations [14]. A wind speed of 7 m/s is assumed, resulting in about 45 m wavelength of the corresponding wind sea. The wind is assumed to blow in an easterly direction, as confirmed by weather charts. Fig. 4(a) shows the wave spectrum with a significant wave height of 1 m, used as input for the forward model.

The first imaging mechanism to be taken into account in the InSAR simulation process is the scanning distortion, which is basically a shearing of the imaged ocean waves due to finite radar platform velocity. As the ocean wave phase speed c_{ph} for a given water depth is known theoretically, this effect can be readily simulated by applying the following transformation in the spectral domain:

$$k_x' = k_x - \frac{c_{ph}}{V}\,|k| \tag{17}$$

$$k_y' = k_y. \tag{18}$$

The experiment was undertaken in an area of about 30 m water depth. Fig. 4(b) shows a single realization of the ocean surface computed from the JONSWAP spectrum. The ocean surface was calculated using a random generator, assuming Gaussian distribution of the Fourier coefficient amplitudes and uniform distribution of the corresponding phases.

Let the Fourier representation of the sea surface elevation η be given by

$$\eta(x) = \sum_k \eta_k\, e^{ikx} + \text{complex conjugate}. \tag{19}$$

The radar cross section σ, which is assumed to be a linear function of the surface elevation, is then calculated from

$$\sigma(x) = \hat{\sigma}\,\left(1 + \sum_k T_k^{\mathrm{RAR}} \eta_k\, e^{ikx} + \text{complex conjugate}\right) \tag{20}$$

where $\hat{\sigma}$ is the spatially averaged cross section. The relation between η_k and the the ocean wave spectrum F is

$$F_k = 2\,\langle \eta_k^*\, \eta_k \rangle. \tag{21}$$

T^{RAR} is the real aperture radar modulation transfer function (RAR MTF), which is commonly split into three parts, the tilt MTF T^{tilt}, the hydrodynamic MTF T^{hydr}, and the range bunching MTF T^{rb} [4]

$$T^{\mathrm{RAR}} = T^{\mathrm{tilt}} + T^{\mathrm{hydr}} + T^{rb}. \tag{22}$$

The following analytical expressions were used for the simulations [1]:

$$T_k^{\mathrm{tilt}} = -\,4\,i\,k_y\,\frac{\cot\theta}{1-\sin^2\theta} \tag{23}$$

$$T_k^{\mathrm{hydr}} = 4.5\,k\,\omega\,\frac{\omega - i\,\mu}{\omega^2+\mu^2}\,\frac{k_y^2}{k^2} \tag{24}$$

$$T_k^{rb} = -\,i\,k_y\,\frac{\cos\theta}{\sin\theta}. \tag{25}$$

Here, ω is the ocean wave frequency, θ the incidence angle, and μ the hydrodynamic relaxation rate, which was chosen as 0.9 s^{-1} following a study by Plant [15]. The orbital velocities and accelerations of the backscattering facettes, u_r and a_r are calculated using the corresponding transfer functions T^v and T^a given by [1]

$$T_k^v = \omega\,\left(\sin\theta\,\frac{k_y}{k} - i\,\cos\theta\right) \tag{26}$$

$$T_k^a = -\,\omega\,T_k^v. \tag{27}$$

The across-track interferogram is then derived using (12). The height model is calculated from the interferogram by subtracting a linear phase introduced by the flat earth (fringe frequency) [10]. Because of the small ocean wave slope, phase unwrapping is not necessary. Setting the baseline components B_y, B_z to zero, (12) is also used to simulate the conventional SAR intensity image [14].

Fig. 4 shows the calculated intensity image Fig. 4(c) and the corresponding bunched DEM Fig. 4(d). The shift and smearing of image points in flight direction is clearly visible in the SAR image as well as in the DEM.

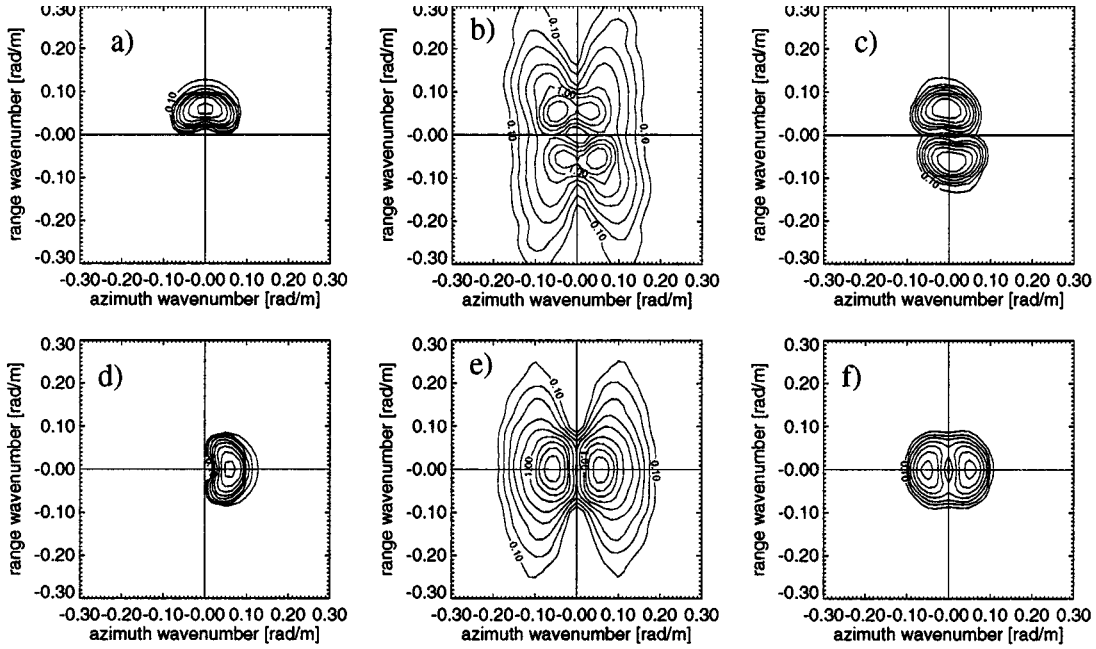

Fig. 5. (a) Across-track InSAR simulation for a 100 m swell system with 0.5 m wave height propagating in range and (d) azimuth direction. (b) Simulated SAR intensity image spectra for swell travelling in range direction and (e) azimuth direction. (c) Simulated bunched DEM spectra (multiplied by two) for swell travelling in range direction and (f) in azimuth direction.

In the framework of linear Gaussian wave theory, the JONSWAP spectrum shown in Fig. 4(a) is a complete statistical description of sea state [16]. In order to calculate the corresponding statistics of the InSAR data, a Monte Carlo method is applied [14], averaging the spectra of bunched DEM and SAR image derived from 40 realizations of the sea surface.

To demonstrate the basic features of the across-track InSAR model, forward simulations were performed with swell and wind sea systems propagating in azimuth and range direction. For the wind sea a fully developed JONSWAP spectrum assuming 7 m/s windspeed is used. Swell is modeled with a JONSWAP spectrum as well, based on parameters settings used in [14].

The dependence of the bunched DEM on scene coherence time is studied, using scene coherence times $\tau_s = 0.12$ s, and $\tau_s = 0.05$ s as in [17].

In the first case the coherence time is slightly longer than the integration time of 0.1 s, while it is shorter in the second case.

Across-track InSAR simulations for swell are presented in Fig. 5(a). Fig. 5(a) and (d) show ocean wave spectra representing swell systems of 100 m wavelength and 0.5 m wave height propagating in range and azimuth direction respectively. The corresponding simulated SAR intensity image spectra and bunched DEM spectra are shown in Fig. 5(b), (c), and (e), (f), respectively. Isolines are logarithmically spaced with five isolines per decade. The units of the isoline labels is m^4 for the ocean wave spectra and bunched DEM spectra and m^2 for the intensity image spectra. To achieve a better comparison between the isolines of the bunched DEM spectra and the wave spectra, the bunched DEM spectra were multiplied by two before plotting. By doing so, the symmetry of the bunched DEM spectrum is taken into account. It can be seen that the distortion of the bunched DEM is weak for the swell case [Fig. 5(c), (f)]. The slight asymmetry of the bunched DEM spectrum with respect to the range axis is due to the scanning distortion mechanism. The swell is also visible in the SAR intensity image [Figs. 5(b), (e)]. However, considerable distortions can be found for the range travelling case Fig. 5(b).

Fig. 6 shows the InSAR simulations for wind sea systems, propagating in range and azimuth direction, respectively. The wind sea spectra with 45 m wavelength and 1 m wave height are shown in Fig. 6(a) and (d). The corresponding simulated SAR intensity image spectra and bunched DEM spectra are shown in Figs. 6(b), (c) and (e), (f). It can be seen that for wind seas the distortions of the bunched DEM become very strong. In particular, for the azimuth travelling wind sea the low pass filtering of the bunched DEM is clearly visible.

The results of the forward simulations with respect to the significant wave height are summarized in Table II. A comparison between ocean wave height HS and corresponding bunched DEM wave heights $\overline{HS}$ for different JONSWAP spectra characterized by wavelength λ and propagation direction ϕ (anticlockwise with respect to flight direction) is presented. In addition the scene coherence time τ_s used for the simulation is given. As already suggested by the bunched DEM spectra in Fig. 5, the estimated wave height $\overline{HS}$ shows reasonable agreement with the true wave height HS in the case of swell. However, for the wind sea $\overline{HS}$ is significantly lower. This effect becomes even stronger for shorter scene coherence times.

As there is no ground truth available for the experiment conducted, no attempt is made to achieve a perfect reproduction of the observation with the across-track InSAR forward model. This would be a complex inversion problem requiring some sort *a priori* information on the high frequency part of

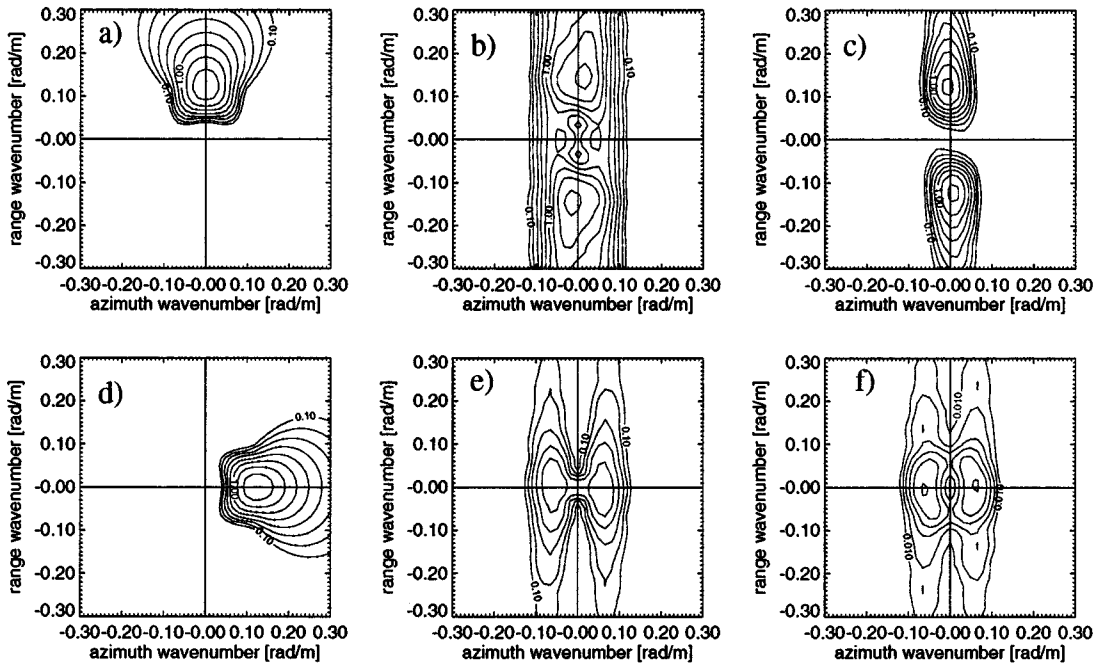

Fig. 6. (a) Across-track InSAR simulation for a 45 m wind sea system with 1 m wave height propagating in range and (d) azimuth direction. (b) Simulated SAR intensity image spectra for range wind sea and (e) azimuth wind sea. (c) Simulated bunched DEM spectra (multiplied by two) for range wind sea and (f) azimuth wind sea.

TABLE II
PARAMETERS OF THE ACROSS-TRACK INSAR SIMULATIONS. THE WAVELENGTH AND PROPAGATION DIRECTION (ANTICLOCKWISE WITH RESPECT TO FLIGHT DIRECTION) OF THE JONSWAP OCEAN WAVE SYSTEMS ARE DENOTED BY λ AND ϕ. THE CORRESPONDING SIGNIFICANT WAVE HEIGHT HS IS GIVEN AS WELL AS THE SCENE COHERENCE TIME τ_s USED IN THE INSAR MODEL. THE LAST COLUMN CONTAINS THE WAVE HEIGHT $\overline{HS}$ ESTIMATED FROM THE BUNCHED DEM

λ [m]	ϕ[°]	HS [m]	τ_s [s]	$\overline{HS}$ [m]
swell				
100	0°	0.5	0.12	0.43
100	90°	0.5	0.12	0.48
100	0°	0.5	0.05	0.36
100	90°	0.5	0.05	0.43
wind sea				
45	0°	1	0.12	0.23
45	90°	1	0.12	0.68
45	0°	1	0.05	0.18
45	90°	1	0.05	0.67
45	90°	2	0.12	1.6

the 2-D wave spectrum [5]. However comparing the simulations shown in Fig. 6(b) and (c) with the observed spectra in Fig. 3(c) and (d). Good agreement can be found for the SAR intensity image spectrum. The simulated bunched DEM spectrum however has a smaller azimuthal width and also a smaller $\overline{HS}$ value than the observation. Simulations showed that an $\overline{HS}$ value of 1.6 m, which is in reasonable agreement with the observed value of 1.9 m, can be obtained assuming a

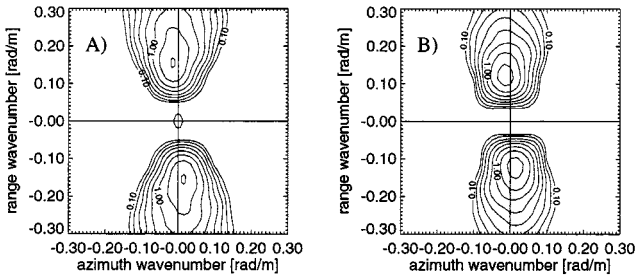

Fig. 7. Across-track InSAR simulation for a 45 m windsea system (HS: 1 m) travelling in range direction, with orbital velocity u_r and acceleration a_r set to zero. (a) Conventional SAR intensity image spectrum and (b) the bunched DEM spectrum.

growing wind sea travelling in range direction with 2 m wave height (compare Table II).

To analyze the impact of sea surface motion on the across-track InSAR model, simulations were carried out with u_r and a_r set to zero. The SAR intensity image spectrum and bunched DEM spectrum obtained for the range travelling wind sea are shown in Fig. 7(a) and (b). Comparing these results with Fig. 6(b) and (c), it becomes obvious that u_r and a_r are the dominant factors in the azimuthal low pass filtering of the bunched DEM spectrum. The remaining weak low pass filtering of the bunched DEM spectrum is due to the limited scene coherence time (0.12 s) and azimuthal resolution (10 m). This simulation also reveals the basic advantage of the bunched DEM compared to the conventional SAR image. Even if the motion effects are switched off, the derivation of an ocean wave spectrum from a SAR intensity image still requires exact knowledge of the RAR MTF. The bunched DEM on the other hand provides the ocean surface spectrum right away in this case.

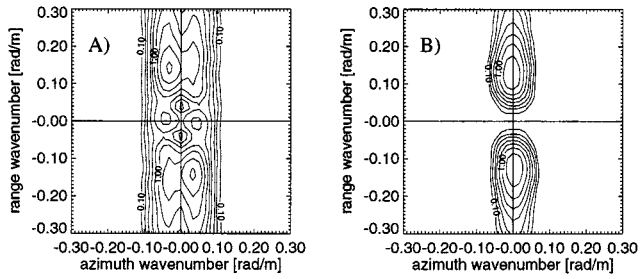

Fig. 8. Across-track InSAR simulation for a 45 m wind sea system (HS: 1 m) travelling in range direction with radar cross section σ_0 assumed as constant. (a) Conventional SAR intensity image spectrum and (b) bunched DEM spectrum.

To study the impact of the real aperture radar modulation on the across-track InSAR model, simulations were performed assuming a constant radar cross section σ. The SAR intensity image spectrum and bunched DEM spectrum obtained for the range travelling wind sea are shown in Fig. 8(a), (b). Comparing the SAR intensity spectrum with the spectrum shown in Fig. 6(b), it can be seen that the RAR modulation mechanism has a strong influence in this case. Figs. 6(c) and 8(b) on the other hand show that the bunched DEM spectrum is less sensitive to the RAR modulation mechanism.

V. Conclusions

The ocean wave imaging capability of high precision airborne across-track InSAR systems has been demonstrated. A theory for the imaging mechanism which is consistent with classical theories for conventional SAR ocean wave imaging was developed. Forward simulations were performed and compared to observations. It turned out that sea surface elevation models derived from across-track InSAR are distorted by motion effects in a similar way as conventional SAR imagery.

It was shown that a straightforward estimation of wave height from the bunched DEM is only feasible for low amplitude swell giving errors of about 10% depending on propagation direction and scene coherence time. Simulations also showed that the distorted DEM is less dependent on the real aperture radar mechanism than conventional SAR images. Therefore, bunched DEM's seem to be an interesting starting point for new ocean wave spectra retrieval algorithm.

A proper validation of the presented theory will be carried out using SAR interferometry experiment for validation of ocean wave imaging model (SINEWAVE) data. In this experiment, the InSAR was flown in a five-legged star shape pattern at three different heights with simultaneous measurements taken by a directional wave rider buoy and the ERS-2 SAR.

Acknowledgment

The authors would like to thank Aero-Sensing Radarsysteme GmbH, Oberpfaffenhofen, Germany, for providing the across-track InSAR data.

References

[1] K. Hasselmann and S. Hasselmann, "On the nonlinear mapping of an ocean wave spectrum into a synthetic aperture radar image spectrum," *J. Geophys. Res.*, vol. 96, pp. 10 713–10 729, 1991.

[2] K. Hasselmann, R. K. Raney, W. J. Plant, W. Alpers, R. A. Shuchman, D. R. Lyzenga, C. L. Rufenach, and M. J. Tucker, "Theory of aperture radar ocean imaging: A MARSEN view," *J. Geophys. Res.*, vol. 90, pp. 4659–4686, 1985.

[3] D. R. Lyzenga, "An analytic representation of the synthetic aperture radar image spectrum for ocean waves," *J. Geophys. Res.*, vol. 93, pp. 13 859–13 865, 1988.

[4] W. R. Alpers, D. B. Ross, and C. L. Rufenach, "On the detectability of ocean surface waves by real and synthetic aperture radar," *J. Geophys. Res.*, vol. 86, pp. 6481–6498, 1981.

[5] S. Hasselmann, C. Brüning, K. Hasselmann, and P. Heimbach, "An improved algorithm for the retrieval of ocean wave spectra from synthetic aperture radar image spectra," *J. Geophys. Res.*, vol. 101, pp. 16 615–16 629, 1996.

[6] C. Melsheimer, M. Bao, and W. Alpers, "Imaging of ocean waves on both sides of an atmospheric front by the SIR-C/X-SAR multifrequency synthetic aperture radar," *J. Geophys. Res.*, vol. 103, pp. 18 839–18 849, 1998.

[7] M. Bao, C. Brüning, and W. Alpers, "Simulation of ocean wave imaging by an along-track interferometric synthetic aperture radar," *IEEE Trans. Geosci. Remote Sensing*, vol. 35, pp. 618–631, May 1997.

[8] L. Shemer, M. Marom, and D. Markam, "Estimates of currents in the nearshore ocean region using interferometric aperture radar," *J. Geophys. Res.*, vol. 98, pp. 7001–7010, 1993.

[9] R. E. Carande, "Estimating ocean coherence time using dual-baseline interferometric synthetic aperture radar," *IEEE Trans. Geosci. Remote Sensing*, vol. 32, pp. 846–854, July 1994.

[10] R. Bamler and P. Hartl, "Synthetic aperture radar interferometry," *Inv. Probl.*, vol. 14, pp. R1–R54, 1997.

[11] R. Bamler, M. Eineder, and H. Breit, "The X-SAR single-pass interferometer on SRTM: Expected performance and processing concept," in *Proc. EUSAR*, 1996.

[12] J. Moreira, "Design of an airborne interferometric SAR for high precision DEM generation," *Int. Arch. Photogramm. Remote Sens.*, vol. 31, pp. 256–265, 1996.

[13] C. T. Swift, "Synthetic aperture radar imaging of moving ocean waves," *IEEE Trans. Antennas Propagat.*, vol. AP–27, pp. 725–729, 1979.

[14] C. Brüning, W. Alpers, and K. Hasselmann, "Monte-Carlo simulation studies of the nonlinear mapping of a two dimensional surface wave field by a synthetic aperture radar," *Int. J. Remote Sensing*, vol. 11, pp. 1695–1727, 1990.

[15] W. J. Plant, "A relationship between wind stress and wave slope," *J. Geophys. Res.*, vol. 88, pp. 1961–1967, 1982.

[16] O. M. Phillips, *Dynamics of the Upper Ocean*. Cambridge, U.K.: Cambridge Univ. Press, 1977.

[17] M. Bao, "On the imaging of a two-dimensional ocean surface wave field by an along-track interferometric synthetic aperture radar," Ph.D., Univ. Hamburg, Hamburg, Germany, 1995.

[18] D. E. Hasselman, M. Dunckel, and J. A. Ewing, "Directional wave spectra observed during JONSWAP, 1973," *J. Phys. Oceanogr.*, vol. 10, pp. 1264–1280, 1980.

Johannes Schulz-Stellenfleth received the Diploma degree in applied mathematics from the University of Hamburg, Hamburg, Germany, in 1996.

He joined the German Aerospace Center (DLR/DFD), Oberpfaffenhofen, Germany, in late 1996. In the framework of the Remote Sensing of Sea Ice (FEME) Project, he worked on SAR observation of ocean waves in the marginal ice zone. He is now a Research Scientist with the Remote Sensing Technology Institute (IMF), DLR. The main interest of his present work is the use of complex SAR data to derive two-dimensional ocean wave spectra. Apart from that, he is working on the application of across-track interferometric (InSAR) data to measure sea surface elevation models.

Susanne Lehner received the M.Sc. in applied mathematics from Brunel University, Uxbridge, U.K., in 1979, and the Ph.D. in geophysics from the University of Hamburg, Hamburg, Germany, in 1984.

She was a Research Scientist with the Max-Planck Institut for Climatology, Hamburg. In 1996, she joined the German Aerospace Center (DLR/DFD) in Oberpfaffenhofen, Germany. Currently, she is a Research Scientist with DLR-IMF, Marine Remote Sensing, Remote Sensing Technology Institute, working on the development of algorithms determining marine parameters from SAR images and the Head of the SAR Oceanography Group. She is a German national delegate of the EU COST action 714, Directional Wave Spectra, Principle and Co-Investigator for ERS1/2 AO2/3 and ENVISAT Programs dealing with the derivation of wind field, ocean wave, and sea ice parameters from ERS SAR images.